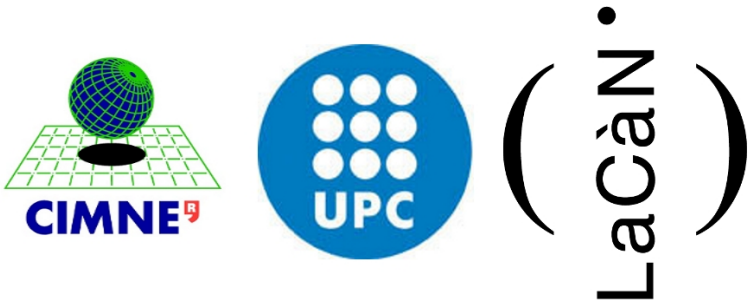

Universitat Politecnica de Catalunya

Erasmus Mundus Master Thesis

Numerical Investigation of Low Reynolds Locomotion

Author:
Flaviu Simon

Advisor:
Prof. Marino Arroyo

June 28, 2013

Acknowledgements

First of all, I would like to thank my advisor, Prof. Marino Arroyo for all the help and guidance he has given me during this process. I can truly say that I have learned a lot from him, and praise him for his patience with me. Additional thanks go to my labmates working in the Laboratori de Calcul Numeric within the UPC who have always been there when I needed help with anything and have made the long days of work less dull.

Then I would like to thank the entire CIMNE and Erasmus Mundus directory who have made it possible for me to study in this prestigios master course.

Last but not least, I would like to thank my family, friends and classmates who have encouraged and supported me during the process of writing my thesis. Without the confidence inspired by them, I would have never been able to go through with this endeavor.

Abstract

The euglenids are microorganisms which are part of the Protista kingdom of eukaryotes. They can be found in diverse aquatic mediums such as ponds, puddles or even the sea, depending on the species. They feed through phagotrophy, phototrophy and osmotrophy. The outer layer of the euglenids is called pellicle and it is flexible, allowing the organism to move and at the same time retaining its original shape.

In my thesis, I have focused on the movement of the green euglena in a low Reynolds number medium, by altering its shape, called metaboly. Although all species use flagella to propell them through the fluid, we will only study the metaboly and its added effect to the locomotion. This type of locomotion has not been fully unravelled, and there remain many questions regarding the actuation mechanism as well as the efficiency of this kind of movement, compared to the largely discussed ciliary and flagellar motions.

Shape changes are actuated by molecular motors on the pellicle, which produce in-plane shear deformations. These shear deformations cannot be accommodated by the pellicle unless it deforms. In a previous work [1], the actuation shear that in vivo euglenids perform has been measured from movies using a kinematical theory of the pellicle. Here, inspired by the spaciotemporal patterns of pellicle shear of real euglenids, and to analyze this shape morphing principle, I consider a simplified pellicle shape, and actuate it with synthetic shear distributions.

Then, I place the motile artificial pellicles in a viscous fluid in the limit of vanishing Re to analyze the hydrodynamic performance as a micro-swimmer. I compare the performance of several actuation pellicle distributions. Further steps in this direction may result in new concepts for microfluidics, for instance in the case of peristaltic micropumps.

The results I obtained reflect the very volatile nature of the pellicle. They also agree with the research that has been done before on this topic: the more shear exists on the pellicle, the more the euglenoid moves forward. My numerical analysis on the kinematics of the pellicle has given insight on the pellicle helicity, and has provided data for the hydrodynamics solution.

Contents

List of Figures

Chapter 1

Introduction

Today there is a constant need for science to explore the microscale and nanoscale world, to try to discover things which could improve fields such as medicine, computational sciences, physics and ultimately, our lives. Analyzing the locomotion at a low Reynolds number can join loose ends in the current view on such microorganisms as the euglenoid, whose *metaboly* has never been fully understood, especially since scientists still don't know what the molecular motor that powers this strange motion is.

My take on low Reynolds number locomotion, which has been almost entirely numerical, is presented in this thesis report. Leaving the numerics aside for a moment, I have to admit that the problem has fascinated me ever since I first saw a recording of the motion. I was amazed of how this minute organism could develop such a complex apparatus necessary for performing this type of locomotion. Finding out more about how this was possible was my incentive when I decided to get involved in this project. Little did I know what I had gotten myself into.

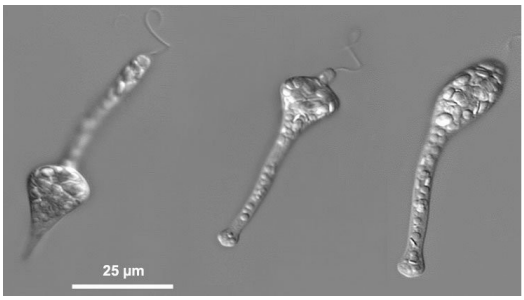

Figure 1.1: Euglenoid metaboly, image adapted from Leander [5]

One approach to studying this movement was done in the article by Arroyo *et al.* [1]. The experiments behind this article are the basis for my numerical investigation, as I mentioned in the abstract. The article challenges the existing conceptual models of swimming at low Reynolds number. It explores the pellicle kinematics and hydrodynamics of the stroke using the model developed. It concludes that each euglenoid studied has a different behaviour, showing geometrically distinct strokes.

What I am trying to understand is the relationship between the pellicle shear and the distance travelled. We know the euglenid is moving, but one objective is to see which velocity it employs and what the efficiency of its movement is. Pellicle deformations are determined by the sliding of pellicle strips, which retain their length and width, as known from previous studies. This is why the surface area of the euglenids remains almost constant during the metaboly, with deviations of 5%.

My study aims to further explore the locomotion of the euglenid, by building a simplified model, recording the relevant results and presenting it in a comprehensible way. The utility of this research is related to the field of microfluidics, taking into account the fact that the pellicle can be a model for engineered active surfaces. A good example of this is the actuators in a peristaltic micropump used for biomedical applications.

Chapter 2

Background

2.1 Theory

In this section I have firstly given an overview on low Reynolds number flow. Also, I have reviewed the biological details of the euglenids, especially those of the pellicle.

2.1.1 Low Reynolds number locomotion

The Reynolds number for an incompressible Newtonian fluid with density ρ and viscosity η, is a dimensionless quantity which qualitatively captures the characteristics of the flow regime obtained by solving the Navier Stokes equations. These need to be solved for the flow field u and the pressure p. [1]

$$\frac{\partial \mathbf{u}}{\partial t}(\rho) + (\rho)(\mathbf{u} \cdot \nabla)\mathbf{u} = -\nabla p + \eta \nabla^2 \mathbf{u}$$

$$\nabla \cdot \mathbf{u} = 0$$

The first equation then becomes, in the low Reynolds number limit:

$$-\nabla p + \eta \nabla^2 \mathbf{u} = 0 = \nabla \cdot \sigma$$

where σ is the stress tensor. The fact that there is no explicit time dependence in the equations means that a self-propelled object has to be subject of a cyclic deformation in shape pace which does not retrace its path. This means that reciprocal motions are not allowed.[2]

[1] Lauga E., *"The hydrodynamics of swimming miorganisms"* , *Rep. Prog. Phys.*, vol.72, no. 15,p.6

[2] Stone H. A, Samuel A.D.T. *"Propulsion of microorganisms by surface distortions"* , *Phys Rev Lett*, vol.77, no. 19, 1,p. 1

There are many physical interpretations of the Reynolds number, such as:

- ratio of the typical inertial terms in the Navier-Stokes equation, to the forces per unit volume.
- ratio of time scales.
- ratio of forces on the body.
- etc.

We can consider the case of a swimmer which deforms its surface for the sole purpose of moving through a fluid, lacking the intervention of external forces. This example perfectly illustrates the case of an euglenoid. Establishing that the mass is m, size is L, velocity is U and the density and viscosity of the fluid are ρ and η, we get the formula for the Reynold's number expressed as:

$$Re = \rho UL/\eta \tag{2.1}$$

The motion at a low Re number is basically a motion without considering inertia, due to its minuteness. This means that the strategies of swimming used by large organisms, such as mammals and fish will not be available for microorganisms living in a low Re medium. In this kind of medium, the forces acting in a precise moment determine what is happening to the microorganism in that moment, without having any effect in the future. The Re number for a microorganism such as the euglenoid is about $10^{-4} - 10^{-5}$, which, when applied to a human being, would be something like swimming in a pool full of molasses and not being able to move more than $1cm/min$, as a famous example by Edward Purcell, a Nobel Prize for Physics winner.[3]

Swimming at a low Reynolds number is done due to a periodic change of shape. A swimming stroke is a closed path in the space of shapes but, in general, an open path in the space of located shapes. If a stroke is small, the shape of the swimmer will not drastically change. Once the stroke is finalized, it will return to its original shape, what differs being the location and orientation. In order to compute the swimming step, X(γ) and the dissipation D(γ), we need to solve the beforeseen Stokes equations for the velocity field $\mathbf{u}$ of the ambient liquid, subject to the boundary conditions that $\mathbf{u}$ vanishes at infinity and satisfies a no-slip condition on the surface of

[3]Purcell E.M.,*"Life at Low Reynolds Number", Brodylab*, Nov. 2005, Web May 2013,p. 3

the swimmer. To obtain the locomotion we have to look into the condition that the force and torque on swimmer disappear at all times.[4]

On the same note, but extending a bit, I have also worked on the idea of optimal swimming, which implies minimizing the energy dissipated per unit swimming distance, $\frac{D(\gamma)}{X(\gamma)}$, while the average speed $X(\gamma)$ has to be kept fixed. The dissipation per unit length $\frac{D(\gamma)}{X(\gamma)}$ and the velocity $\frac{X(\gamma)}{\tau}$ scale as $\frac{1}{\tau}$, where τ is the period of the stroke. We can define the inefficiency of the stroke, or the swimming drag coefficient in the following way:

$$\delta(\gamma) = \left(\frac{D(\gamma)}{X(\gamma)}\right) / \left(\frac{4\pi\mu X(\gamma)}{\tau}\right)$$

This number is inverse proportional with the efficiency of a swimmer. Because δ in d dimensions has size L^{d-2}, geometrically similar swimmers have the same efficiency in two dimensions, while the smaller swimmers are more efficient in three dimensions.

A slightly different approach to the notion of efficient swimming was that employed by Lighthill. He defines the efficiency of a swimming microorganism as the power that would be needed to drag an object of the same size with the same speed through viscous fluid, divided by the actually dissipated power. This definition of the efficiency could technically generate some values which exceed 100%, but the actual swimming efficiency is of the order of 1%. The internal energy losses are ignored when calculating Lighthill's efficiency. [5]

2.1.2 Overview on pellicle configuration and metaboly

There are many papers discussing life and locomotion at low Reynolds number. What has not been discussed so extensively is the efficiency at which different microorganisms manage to move through this type of fluid. Although metaboly has attracted attention due to its unique characteristics, there are still many questions as to what powers it. My research has also tried to analyze the efficiency of the euglenoid's movement, as some previous experiments show that it is much better than that of other microorganisms. We will see that this efficiency is proportional to the bending shear of the pellicle.

It is known that the shape changes of the euglenoid are enabled by the existence of the pellicle and its subcomponents: the cytoskeleton, prote-

[4]Avron J.E.,Gat O., Kenneth O.*"Optimal swimming at low Reynolds numbers", Phys Rev Lett*, Oct. 2004, Vol. 93, No. 18,p. 1

[5]Osterman N.,Vilfan A.,*"Finding the ciliary beating pattern with optimal efficiency", PNAS*, Sept. 2011,Vol. 108, No. 38,p. 1

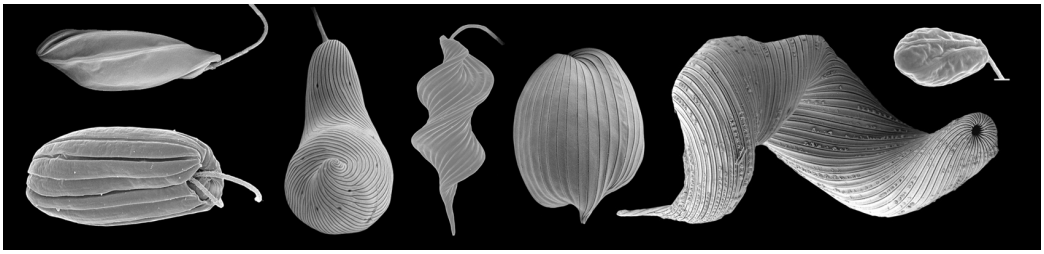

Figure 2.1: Different pellicle shapes for euglenoids, image adapted from Leander [5]

naiceous strips, microtubules, plasma membrane, and the tubular cisternae. This complex system is considered as a synapomorphy within the evolution of this class of eukaryotes. Different species of euglenoids have different pellicle configurations. Some euglenoids exhibit a pellicle with few strips, arranged longitudinally. This type of pellicle is quite rigid, the strips being oftentimes fused together, preventing metaboly. When strips are arranged in a helical manner however, the microorganism can display metaboly.

Focusing on the strips, we denote the fact that they are composed of a type of proteins known by the name of *articulins*, and generally have an S-shaped cross-section which consists of two regions: an arch region and a heel region. The adjacent strips basically fit together along their lateral edges by overlapping ones arch with the other's heel. The discontinuities generated by this type of articulation enable the dynamic changes in the cell shape as well as the cytoskeletad replication preceding the cell division. In some lineages, there are so called projections on the frame of the strips which help join it with its neighbour, as seen in Fig. 2.2. These can be differentiated in pre-articular and post-articular projections, based on their position within the joint. The robustness of these varies greatly with the different species of euglenoids. The thinner they are, the more flexible the pellicle is during metaboly. [6]

The strips also have a vital role in the duplication of euglenoids, or cytokinesis. The number of strips doubles before this process starts, new strips emerging in the articulation zones between mature strips. In some lineages, these new strips do not extend up to the posterior end of the cell, which determines the formation of the so-called whorls of reduction. The whorls will have a different number for different species, ranging from 1 to 4.

[6]Leander B.S., *"Euglenida: euglenids or euglenoids"* , Version 11, September 2008, .http://tolweb.org/Euglenida/97461¿

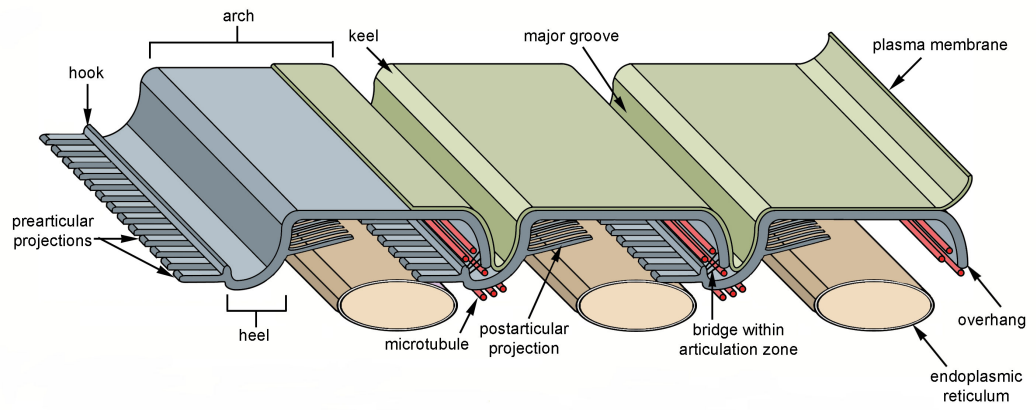

Figure 2.2: Pellicle configuration, image adapted from Leander [5]

The history of how the pellicle evolved in the case of euglenids is quite interesting and shows how in many cases, a change in the mode of nutrition has determined a change in the number of pellicle strips as well as the way they are oriented. Euglenids that prey on small cells will have less than 12 rigid strips, while euglenids that consume large cells will have 20 to 60 strips capable of metaboly.[7]

It is considered that euglenoids may provide information about the evolution of unicellular eukaryotes. This is because they are among the few protists that possess diverse morphological traits that appear to be controlled by a common developmental mechanism, the details of which are completely unknown at this time.[8]

By observing one species of euglenoid called Euglena fusca which possesses a large number of strips and highly ornamented cells, we conclude that during the shape changes of the pellicle, the strips do not change their length or width, but the helicity. The active motions of the pellicle are thought to be fueled by ATP, but there is no certain response as to what kind of molecular motor is employed in this action.

Many other questions which are not fully elucidated arise regarding the pellicle's conformation and behaviour, such as the the appearance of pellicular knobs on random strips and their role. It seems like the different strip surface patterns are an effect of constructive neutrality or evolutionary history rather than adaptation to the environment. I will not further discuss

[7] *Idem*

[8] Leander B.S., *"Trends in the evolution of the euglenid pellicle", Evolution*, April. 2001, vol. 55, no. 11,p. 1

these matters, because it would sidetrack me from my original goal of strictly analyzing the metaboly from a mechanical point of view and illustrating its advantages for the euglenoids.

The model I have proposed for the pellicle kinematics is directly based on the connection between distributed actuation and shape changes.[9]

[9]M. Arroyo,L. Heitai,D. Millan and A. DeSimone, *"Reverse Engineering the Euglenoid Movement"*, PNAS, October 30, 2012,vol. 109 no. 44.,p. 2

Chapter 3

Kinematics of the metaboly

3.1 Obtaining the mathematical expressions

3.1.1 Pellicle surface and generating curve

This chapter numerically illustrates the motion of the pellicle. We have the initial spline curve written in the following way:

$$c_a(u) = \sum_{I=1}^{N} B_I(u)\{r_I, z_I\}_a \tag{3.1}$$

In this relation $B_I(u)$ are the basis functions referred to a reference interval u $\in$ [0,1] and $\{r_I, z_I\}_a$ are the cylindrical coordinates of the control points associated with the a-th frame. Isomap embeds each frame in a point τ in a periodic segment scaled to [0,1]. The generating curve of the pellicle is then parametrized in pseudo-time as:

$$c_a(u) = \sum_{I=1}^{N} B_I(u) \sum_{a=1}^{n} w_a\{r_I, z_I\} \tag{3.2}$$

where n is the number of frames, and $w_a(\tau)$ are smooth meshfree maximum-entropy basis functions.[10]

The stroke path is given by $\boldsymbol{\tau}(\tau) = \sum_{a=1}^{n} w_a(\tau)\boldsymbol{\tau}_a$. By minimizing $|\boldsymbol{\tau}(\tau) - \boldsymbol{\tau}_a|^2$ we find the pseudo-instant for each frame associated to the time instant $(a-1)\Delta t$.

[10]M. Arroyo,L. Heitai,D. Millan and A. DeSimone, *"Reverse Engineering the Euglenoid Movement: Suporting information"*, PNAS, October 30, 2012,vol. 109, no. 44., p. 1

The pellicle deforms due to simple shear γ, the part of the total area which measures a given parallel. The generating curve (r_0 and z_0) can be differentiated with regards to time in order to obtain the pellicle velocities within the symmetry plane. The orientation is given by the vector field along the strips s_0, and the surface meridian α_0. C is then the Cauchy-Green deformation tensor which characterizes the strain of the pellicle surface in the reference configuration.[11]

If c(u,t) = $\{r(u,t), z(u,t)\}$ is the generating curve of the axisymmetric surface Γ. The speed a is equal to $\sqrt{r'^2 + z'^2}$, containing the partially differentiated components of the generating curve. $n = 1/a\{-z', r'\}$ is the unit normal. The element of area of the axisymmetric surface can be expressed as $dS = 2\pi ardu$. Summing everything up, we get the following expressions for the area and volume:

$$S = 2\pi \int_0^1 ardu, V = \frac{1}{3}\int_\Gamma x \cdot ndS = \frac{2\pi}{3}\int_0^1 (-z'r + r'z)rdu \tag{3.3}$$

3.1.2 Deformation of the pellicle

Based on what I have discussed in the previous section, the reference pellicle configuration can be formulated as $x_0(\theta) = \{r_0\cos(\theta), r_0\sin(\theta), z_0\}$. In the previous formula, the azimuthal angle $\theta \in [0, 2\pi]$ refers to material particles. $r(t)$, $z(t)$ and $\psi(t)$ represent the full prescription of the pellicle Lagrangian motion along the stroke, as stated in the article.[12]

$$x(\theta, t) = \left\{ \begin{array}{c} r(t)\cos[\theta + \psi(t)] \\ r(t)\sin[\theta + \psi(t)] \\ z(t) \end{array} \right\} \tag{3.4}$$

In Cartesian coordinates, the natural basis vectors of the tangent place to the deformed configuration are:

$$x = \left\{ \begin{array}{c} r'\cos(\theta + \psi) - r\psi'\sin(\theta + \psi) \\ r'\sin(\theta + \psi) + r\psi'\cos(\theta + \psi) \\ z' \end{array} \right\} \tag{3.5}$$

$$x_\theta = \left\{ \begin{array}{c} -r\sin(\theta + \psi) \\ r\cos(\theta + \psi) \\ 0 \end{array} \right\} \tag{3.6}$$

Because we assume that the local deformation is the result of simple shear along the pellicle strips, the local deformation gradient takes the form:

[11] Arroyo,loc. cit.

[12] *Ibid.*,p. 2

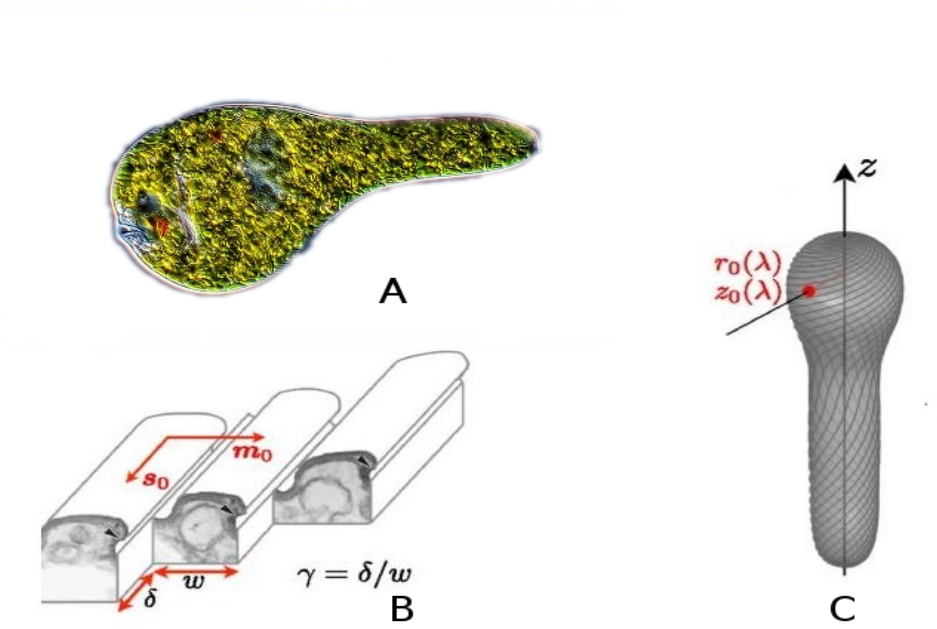

[Pellicle characteristics](A) shows a microscope image of a green euglena[26].(B) shows the sliding between the different pellicle strips which causes the pellicle shear γ. (C) is a depiction of the pellicle and its characteristic reference configuration $\{r_0, z_0\}$. These last two figures were adapted from Arroyo *et al.* [1]

$$F = R(Id + \gamma s_0 m_0^T)$$

where R is the orthogonal matrix, $s_0 = \sin(\alpha_0 e_0) + \cos(\alpha_0 e_{0\theta})$ and $m_0 = -\cos(\alpha_0 e_0) + \sin(\alpha_0 e_{0\theta})$. α_0 is the angle of the pellicle strips with the surface parallels in the reference configuration.

Then we can formulate the Cauchy-Green deformation tensor as:

$$C = F^T F = Id + \gamma(s_0 m_0^T + m_0 s_0^T) + \gamma^2 m_0 m_0^T \tag{3.7}$$

$$= \begin{bmatrix} 1 - 2\gamma \sin(\alpha_0)\cos(\alpha_0) + \gamma^2 \cos^2(\gamma_0) & \gamma(\sin^2(\alpha_0) - \cos^2(\alpha_0)) - \gamma^2 \sin(\alpha_0)\cos(\alpha_0) \\ \gamma(\sin^2(\alpha_0) - \cos^2(\alpha_0)) - \gamma^2 \sin(\alpha_0)\cos(\alpha_0) & 1 + 2\gamma \sin(\alpha_0)\cos(\alpha_0) + \gamma^2 \sin^2(\gamma_0) \end{bmatrix} \tag{3.8}$$

Equating this with the deformation derived from the shape changes, we get relations between the reference pellicle conformation (r_0, z_0, α_0), the de-

formed configuration (r, z, ψ) and the pellicle shear for the reference state (γ):

$$(a^2 + r^2\psi'^2)/a_0^2 = 1 - 2\gamma_0 \sin(\alpha_0)\cos(\alpha_0) + \gamma_0^2 \cos^2(\alpha_0) \tag{3.9}$$

$$(r^2\psi')/(r_0 a_0) = \gamma_0(\sin^2(\alpha_0)\cos^2(\alpha_0)) - \gamma_0^2 \sin(\alpha_0 \cos(\alpha_0) \tag{3.10}$$

$$(r/r_0)^2 = 1 + 2\gamma_0 \sin(\gamma_0)\cos(\gamma_0) + \gamma_0^2 \sin^2(\gamma_0) \tag{3.11}$$

We are making the assumption that $\alpha_0 = \frac{\pi}{2}$, by considering that the pellicle strips are parallel to the meridians. In a time dependent case, the component of the generating curve r(u) is equal to $r_0(u)\sqrt{\gamma(u)^2 + 1}$, where $\gamma(u)$ is the simple shear.

Based on these equations, we can determine the pellicle shear (γ) and the azimuthal displacement (ψ). So from Eq. 3.11 γ is then:

$$(-\cos(\alpha_0) \pm \sqrt{(r/r_0)^2 - \sin^2(\alpha_0)})/\sin(\alpha_0) \tag{3.12}$$

Respectively, from Eqs. 3.10 and 3.11 we deduct the following formulation:

$$\frac{r^2}{a_0 r_0}\psi' = \frac{\cos(\alpha_0)}{\sin(\alpha_0)}\left[1 - \left(\frac{r}{r_0}\right)^2\right] + \gamma_0 \tag{3.13}$$

We assume $\alpha_0 = \frac{\pi}{2}$ and we can then find ψ by integrating this equation. First we obtain ψ':

$$\psi'(u) = \frac{a_0(u)\gamma(u)}{r_0(u)(\gamma(u)^2 + 1)} + \gamma(0) \tag{3.14}$$

Then we get the azimuthal displacement:

$$\psi(u) = \int_0^u \frac{a_0(s)\gamma(s)}{r_0(s)(\gamma(s)^2 + 1)}\, ds + \psi(0) \tag{3.15}$$

For accuracy, we set $\psi(0)$ as 0 so that $\int_\Gamma \psi r dS$ is 0.

If the pellicle strips are parallel to the meridians in the reference configuration, then $\gamma = \sqrt{(r/r_0)^2 - 1}$. What is clear from the expression is that the reference configuration component r_0 is inversely proportional with the pellicle shear γ.[13]

[13] *Ibid.*,p. 4

The third component of the deformed configuration in the time independent case can be obtained from Eq. 3.9 and from the definition of the speed a :

$$z'(u) = \sqrt{\frac{a_0(u)^2 - [(\gamma(u)^2+1)r_0'(u) + r_0(u)\gamma(u)\gamma'(u)]^2}{\gamma(u)^2+1}} \tag{3.16}$$

And then by integrating this we get:

$$z(u) = \int \sqrt{\frac{a_0(s)^2 - [(\gamma(s)^2+1)r_0'(s) + r_0(s)\gamma(s)\gamma'(s)]^2}{\gamma(s)^2+1}}\, ds + z(0) \tag{3.17}$$

The time dependent deformed configuration is then obtained by differentiating the same expressions but with respect to time. So for the component $r(u,t) = r_0(u)\sqrt{\gamma(u,t)^2+1}$, the time derivative is:

$$\dot{r}(u,t) = \frac{r_0(u)\gamma(u,t)\dot{\gamma}(u,t)}{\sqrt{\gamma^2(u,t)+1}} \tag{3.18}$$

Doing the same for the azimuthal displacement ψ and using Eq. 3.13, we get:

$$\psi'(u,t) = \frac{a_0(u)\gamma(u,t)}{r_0(u)(\gamma(u,t)^2+1)} \tag{3.19}$$

Integrating:

$$\psi(u,t) = \int_0^u \frac{a_0(s)\gamma(s,t)}{r_s(s)(\gamma(s,t)^2+1)}\, ds + \psi(0,t) \tag{3.20}$$

And then differentiating with respect to time:

$$\dot{\psi}(u,t) = \int_0^u \frac{a_0(s)(\gamma(s,t)^2-1)\dot{\gamma}(s,t)}{r_s(s)(\gamma(s,t)^2+1)^2}\, ds + \dot{\psi}(0,t) \tag{3.21}$$

Finally, from Eqs. 3.9, 3.11, 3.13, we find the formulas for the third component of the deformed configuration:

$$z'(u,t) = \sqrt{\frac{a_0(u)^2 - [(\gamma(u,t)^2+1)r_0'(u) + r_0(u)\gamma(u,t)\gamma'(u,t)]^2}{\gamma(u,t)^2+1}} \tag{3.22}$$

$$\rightarrow z(u,t) = \int_0^u \sqrt{\frac{a_0(s)^2 - [(\gamma(s,t)^2+1)r_0'(s) + r_0(s)\gamma(s,t)\gamma'(s,t)]^2}{\gamma(s,t)^2+1}}\, ds + \\ + z(0,t) \tag{3.23}$$

The time derivative is then:

$$\dot{z}(u,t) = \int_0^u -\gamma(s,t)\dot{\gamma}(s,t)(a_0(s)^2 - k^2)j(\gamma(s,t)^2+1)^{-1} - (\gamma(s,t)^2+1)k \cdot \\ \cdot [\dot{\gamma}(s,t)(2\gamma(s,t)r_0'(s) + r_0(s)\gamma'(s,t)) + r_0(s)\gamma(s,t)\dot{\gamma'}(s,t)] \cdot \\ \cdot j\, ds + \dot{z}(0,t) \tag{3.24}$$

where k $= [(\gamma(s,t)^2+1)r_0'(s) + r_0(s)\gamma(s,t)\gamma'(s,t)]$
and j $= 1/\left[(\gamma(s,t)^2+1)\sqrt{\frac{a_0(s)^2-[(\gamma(s,t)^2+1)r_0'(s)+r_0(s)\gamma(s,t)\gamma(s,t)]^2}{\gamma(s,t)^2+1}}\right]$

3.1.3 Pellicle velocity

Having the components of the reference and deformed configuration, as well as their derivatives, we can proceed to calculating the pellicle velocity field in the x-z plane:

$$\dot{x} = \left\{ \begin{array}{c} \dot{r} \\ r\dot{\psi} \\ \dot{z} \end{array} \right\} = v_n^s n + ve + v_\theta e_\theta \tag{3.25}$$

In this expression, v_n^s is the normal velocity due to shape changes and is equal to $n \cdot \dot{x} = (-z'\dot{r} + r'\dot{z})/a$, v is the tangential velocity along generating curves (meridians), and is equal to $e \cdot \dot{x} = (r'\dot{r} + z'\dot{z})/a$ with $e = 1/a\{r', 0, z'\}$ and finally $v_\theta = e_\theta \cdot \dot{x} = r\dot{\psi}$ with $e_\theta = \{0, 1, 0\}$, is the tangential velocity along the parallels.[14]

3.2 Software implementation

The practical side of my dissertation, the software implementation of the model, has been done in Matlab. This has accounted for a high percentage of

[14] *Ibid*,p. 5

my work, an evident continuation of the entire theoretical process employed in the project so far.

When I reached this point in my work, I have been provided with a Matlab code by my supervisor, which had been devised by the ones previously working on the article cited under [1].

To get a grasp on the possibilities offered by the code, as well as ease to ease my work, I have simplified the code, adapting it to a more rudimentary geometry which could offer the same results in terms of pellicle shear and deformation. The shape I chose closely resembles that of the original geometry of Euglena Fusca, is a cylinder. The cylinder has been defined by the x, y and z dimensions.

The first part of the code employs a step-by-step approach to obtain the pellicle shear, and uses 3rd degree B-splines to define the Gauss quadrature. The hydrodynamics solver employed by the code in the final part of my dissertation uses the Boundary Integral Method, which is more appropriate and gives successful results in other cases when it was adopted such as the study of hydrodynamics of swimming micro-organisms in the Stokesian regime (Ramia *et al.* 1993; Shum *et al.* 2010). I have presented a detailed description of the equations behind the process of solving the Stokes equation in the previous section.[15]

3.2.1 Simplified pellicle

As I mentioned before, my work on the code has started with a simplification of the pellicle geometry, in order to ease the work and also to see if a very basic geometrical shape would suffice as a foundation for the movement. This is why I have used a cylinder of specific dimensions for the reference state of the pellicle.

The pellicle shear function has been implemented so that it gives the possibility of switching the example and it has been defined over a time interval from 0 to 1. Basically, the cases presented containing the function and its derivative are just examples that I make use of to illustrate the characteristics of the pellicle. As a visual aid, the pellicle shear for the different functions has been plotted in a map which can be seen in Figure 3.2. The functions are:

$$\gamma_{CP1} = amplitude \cdot \sin\left(u_{CP} + t/2\right) \cdot 2 \cdot \pi^2; \tag{3.26}$$

[15]Zhu L., Lauga E., Brandt L., *"Low-Reynolds number swimming in a capillary tube"*, J Fluid Mech, 29 April, 2013,vol 726, pp.285-311

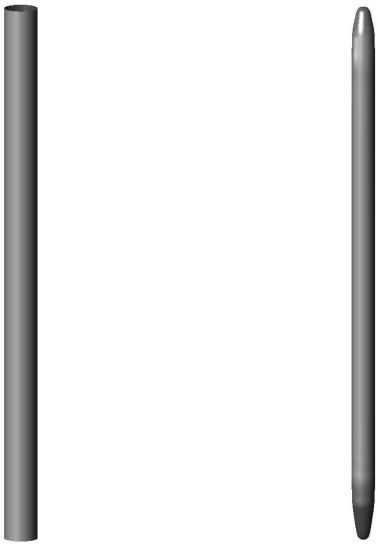

(a) open (b) closed

Figure 3.1: Reference state of the pellicle in the open 3D surface(simplified) form and in the closed 3D surface(complex) form.

$$\dot{\gamma}_{CP1} = amplitude \cdot 2 \cdot \pi \cdot \cos\left(u_{CP} + t/2\right) \cdot 2 \cdot \pi \cdot \sin\left(u_{CP} + t/2\right) \cdot 2 \cdot \pi; \quad (3.27)$$

$$\gamma_{CP2} = amplitude \cdot \sin\left(u_{CP} + t\right) \cdot 2 \cdot \pi; \quad (3.28)$$

$$\dot{\gamma}_{CP2} = amplitude \cdot 2 \cdot \pi \cdot \cos\left(u_{CP} + t\right) \cdot 2 \cdot \pi; \quad (3.29)$$

$$\gamma_{CP3} = amplitude \cdot e^{-k \cdot ((u_{CP} - 0.5) - 0.5 \cdot (t - 0.5))^2}; \quad (3.30)$$

$$\dot{\gamma}_{CP3} = k \cdot ((u_{CP} - 0.5) - 0.5 \cdot (t - 0.5)) \cdot \gamma_{CP}; \quad (3.31)$$

where u_{CP} is a matrix containing the values of the 43 control points in time and t is the time (40 steps in our case) and k is a parameter which is inversely proportional with the width of the bulge .

Moving foward with the Matlab code implementation of the synthetic strokes, the next phase was to compute the shapes along the stroke. The expressions for the components of the deformed configuration (r,z,ψ) are

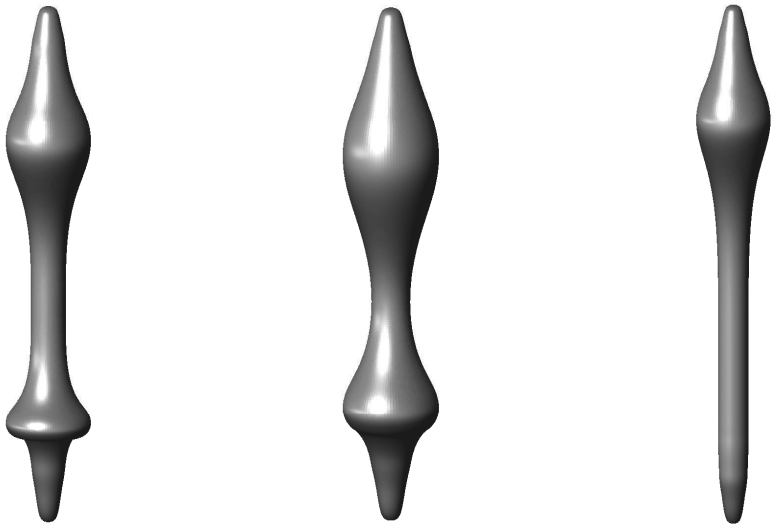

(a) function 1 (b) function 2 (c) function 3

Figure 3.2: The deformed pellicle for the 3 different shear functions. I have mostly experimented with function 3.

given earlier in section 3.1.2. All three parameters are evaluated both at Gauss points and at sample points. Now that I had the expressions relating the pellicle shear, pellicle orientation, shape changes and azimuthal motions, I went on to calculate the velocity components of the pellicle.

The velocity field, as denoted by Eq. 3.25, has been obtained by first computing the components of the three velocities: $\dot{r}$, $\dot{z}$ and $\dot{psi}$. These are the time derivatives of the deformed configuration, as seen in Eq. 3.18, 3.24 and respectively 3.21. The process of differentiation has been described in section 3.1.2. The natural basis function $x(\theta, t)$ has been presented in Eq. 3.4. By differentiating these, I have obtained the velocities, which I have then plotted on the pellicle using the inbuilt Matlab function *quiver3*. This function plots the vector components present in the first 3 arguments at the points given by the last 3 arguments.

The next step in my work was to check for the consistency of my calculations. The analytical results had to be consistent with the numerical results. For this I have computed the values of the velocity through numerical differentiation using the algorithm:

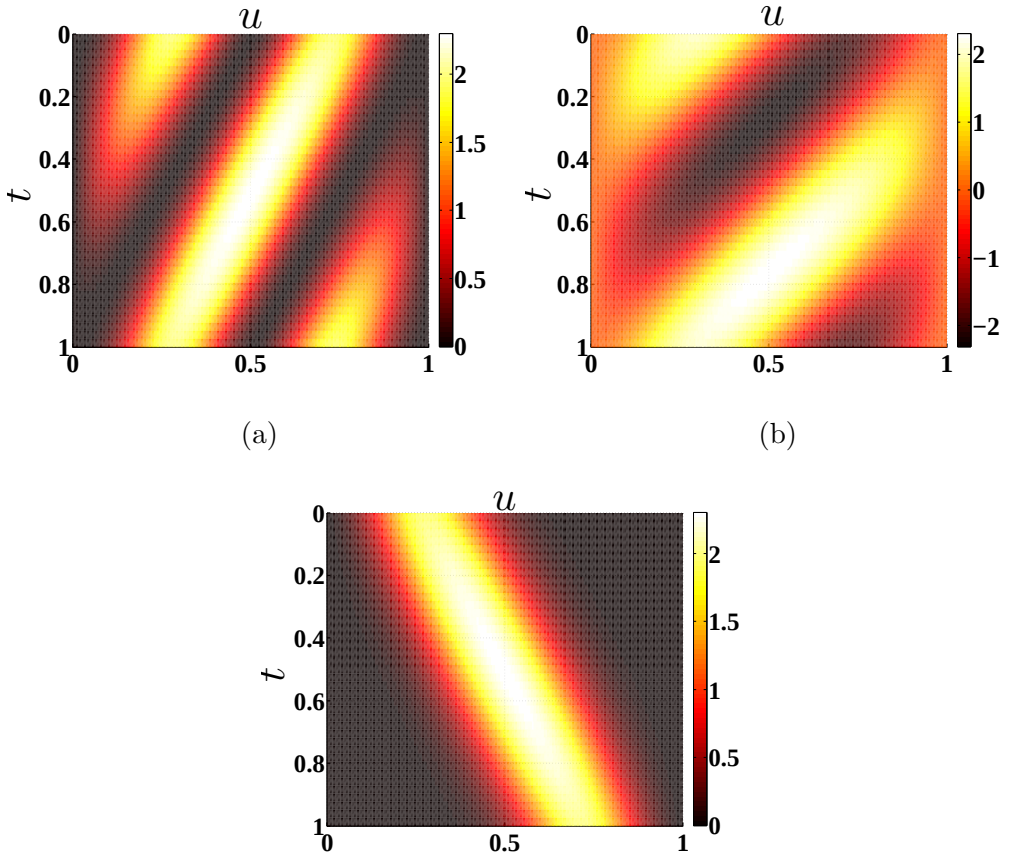

(a) (b)

(c)

Figure 3.3: Map of pellicle shear for the 3 cases. Further in my analysis I have focused on case c.

$$V_x = \frac{(x^{n+1} - x^n)}{\Delta t} \tag{3.32}$$

$$V_y = \frac{(y^{n+1} - y^n)}{\Delta t} \tag{3.33}$$

$$V_z = \frac{(z^{n+1} - z^n)}{\Delta t} \tag{3.34}$$

and the values of the mean velocity:

$$\overline{V}_1 = \frac{(x^{n+1} + x^n)}{2} \tag{3.35}$$

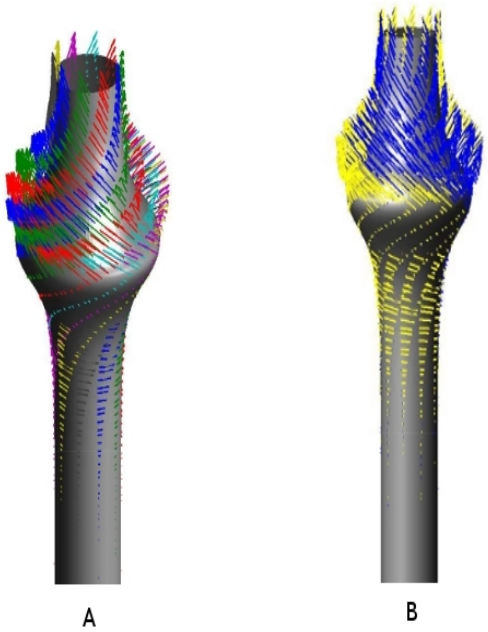

Figure 3.4: (A) An overall image of the velocity vectors plotted with different colors on the 10 pellicle strips. (B) Quiver plot showing the coincidence of the blue and yellow quiver arrows representing the numerical differentiation and the average velocities.

$$\overline{V}_2 = \frac{(x^{n+1} + x^n)}{2} \tag{3.36}$$

$$\overline{V}_3 = \frac{(x^{n+1} + x^n)}{2} \tag{3.37}$$

Having these values, I have plotted with the *quiver3* Matlab function the two sets of velocities in different colors, in order to see whether the arrows are superposed or not. Figure 3.4 shows a detail of this. The values have been plotted at the Gauss points.

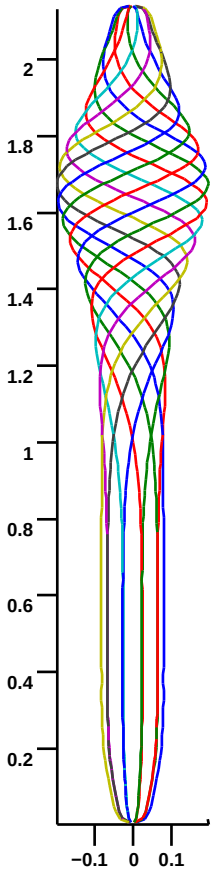

Figure 3.5: 3D line plot of the displacements for every pellicle strip.

3.2.2 Complex pellicle

The cylinder has been a good simplification for the euglenoid pellicle, but as I advanced with my work, I needed a better geometry for this complex mechanism. This is why I developed a different geometry which I used for the rest of the numerical analysis. The new geometry has been defined using a vector which contained a set of data for the initial half-contour. This has been then used to interpolate the generating curve of the axysimmetric surface along with the information obtained by defining the b-splines and

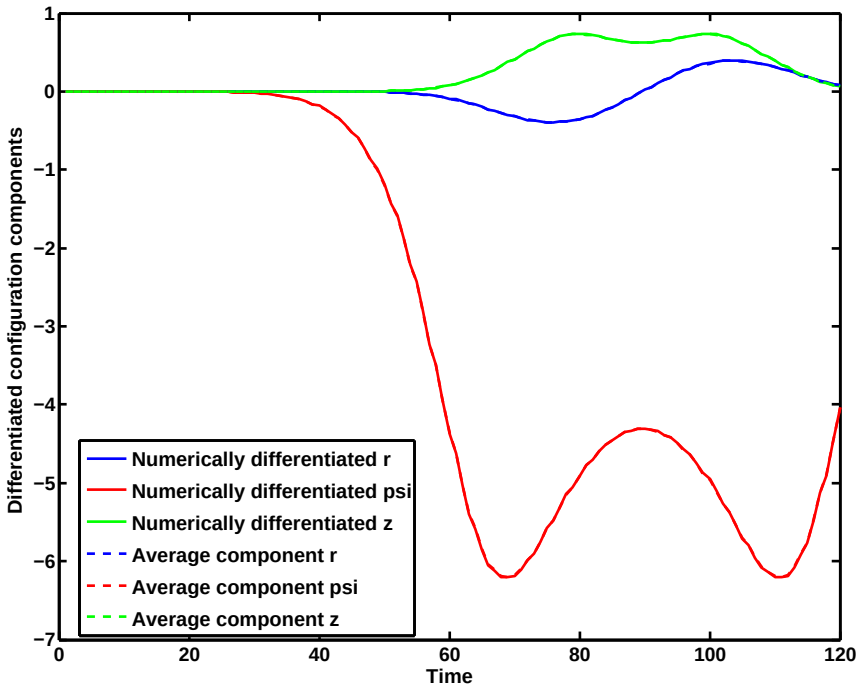

Figure 3.6: Line plot of the 3 velocities both calculated by numerical differentiation and by average

Gauss quadrature. The speed a is the obtained by using the formula available in Section 3.1.1. Then I have followed the steps described in the previous subsection: evaluating the reference shape. What changes here is that we have to use the Least Squares method in order to obtain the control polygon of the deformed surface, by comparing the initial reference pellicle and the new configuration of the pellicle. The Least Squares Method is used to generate an overall solution which minimizes the sum of squares of the errors existent in the results of the equations. Basically this method minimizes the sum of squared residuals to fit data.[16].

[16]Lai T.L., Robbins H., Wei C.Z., *"Strong consistency of least squares estimates in multiple regression"*, Proc Natl Acad Sci USA, 6 July, 1978, Vol. 75, No. 7

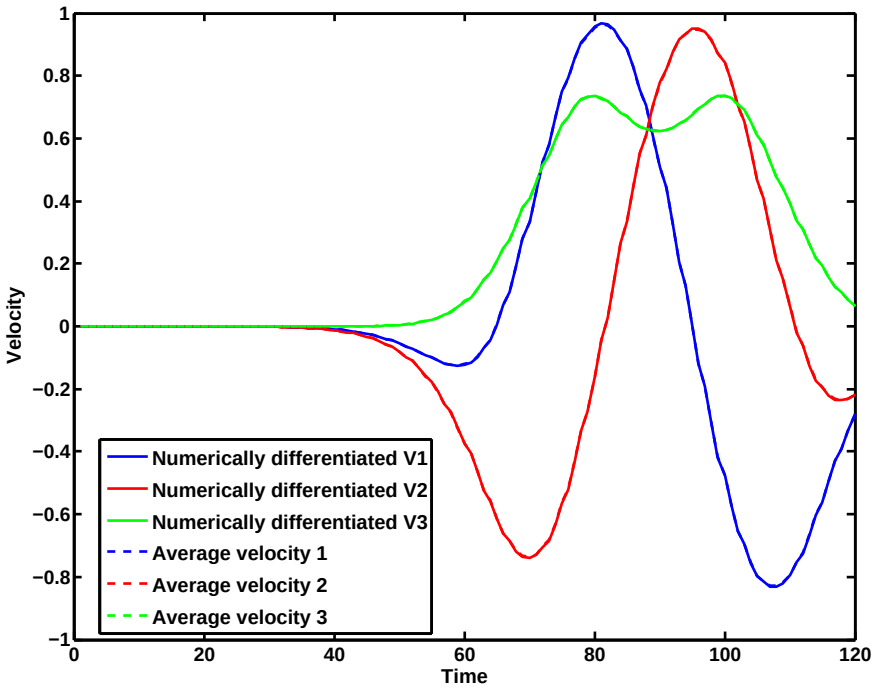

Figure 3.7: Line plot of the 3 velocity components both calculated by numerical differentiation and by average

$$r^h(u) = \sum_I (B_I(u) r_I) \tag{3.38}$$

$$z^h(u) = \sum_I (B_I(u) z_I) \tag{3.39}$$

These are the two components of the pellicle configuration. B_I is the basis function. r_I and z_I are the unknowns. By using the Least Squares Method we then get the following expressions:

$$\min_{r_I} = \frac{1}{2} \int |r^h(u) - r(u)|^2 \, dS \tag{3.40}$$

$$\min_{z_I} = \frac{1}{2} \int |z^h(u) - z(u)|^2 \, dS \tag{3.41}$$

where dS has been defined previously as $2\pi ardu$.
We come to

$$\begin{aligned} I_r &= \tfrac{1}{2}\sum |r^h(u_i g) - r(u_i g)|^2 w_i g \\ &= \tfrac{1}{2}\sum |\sum (B_I(u) r_I) - r(u_i g)|^2 w_i g \end{aligned} \tag{3.42}$$

and

$$\begin{aligned} I_z &= \tfrac{1}{2}\sum |z^h(u_i g) - z(u_i g)|^2 w_i g \\ &= \tfrac{1}{2}\sum |\sum (B_I(u) z_I) - z(u_i g)|^2 w_i g \end{aligned} \tag{3.43}$$

$$M r_I = b \tag{3.44}$$

$$M z_I = b_I \tag{3.45}$$

Where M is the matrix defined as the sum of the basis functions and weights.

$$M_{IJ} = \sum_i g B_I(u_i g) B_J(u_i g) w_i g \tag{3.46}$$

and

$$b_I = \sum_i g B_I(u_i g) r(u_i g) w_i g \tag{3.47}$$

$$b_I = \sum_i g B_I(u_i g) z(u_i g) w_i g \tag{3.48}$$

We have all the required data necessary to perform the regression and obtain r_I, z_I, the components of the control polygon. This is done in the code by a predefined function which also calculates the error.

With the control polygon, we can calculate the new value for the generating curve, by interpolation. This data will be used in the final part of the analysis, the hydrodynamics, when the swimmer is immersed in a newtonian fluid. The Galerkin Boundary Element Method is used to solve the Stokes equation of fluid flow.

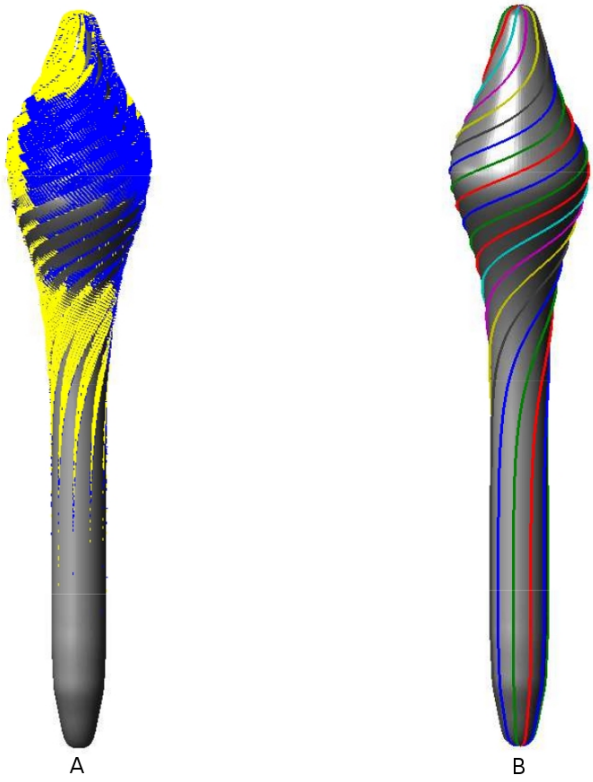

Figure 3.8: The plot shows both the quiver arrows for the numerically differentiated velocity and the average velocity (A) and the pellicle strips and the way they twist during the motion of the microorganism (B).

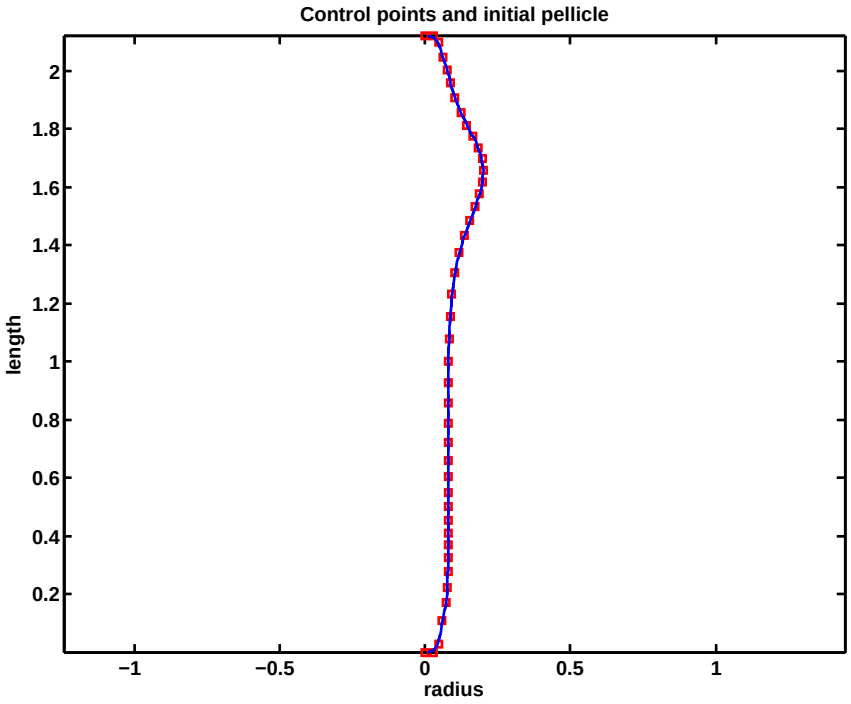

Figure 3.9: The control polygon with red squares reprezenting the 43 control points. The black line which is seemingly connecting the points is the second expression for the generating curve and the dashed line which is not visible is the initial configuration of the pellicle. The distance between the last two parameters I have mentioned is about $1.5 \cdot 10^{-4}$.

Chapter 4

Swimming hydrodynamics

4.1 Obtaining the mathematical expressions

The final part of the project naturally involves placing the swimmer in a fluid, which in our case is Newtonian which means its viscosity does not change with the flow rate. The value for the Reynolds number is estimated to be 10^{-4}, taking into account the size of the euglenids ($50\mu m$) and the stroke frequency (0.1 Hz). The flow is characterized using Stokes equations, as we have seen earlier. They are solved using the Boundary Integral Method, which distinguishes itself from the Finite Element Method through the fact that only domain surfaces need to be meshed. It is the method of choice when solving external problems and those involving complex regions. The dimension of the problem is reduced and integration along complicated curves, if done with care, can be accurately evaluated.

The general integral representation of the Stokes equations is:

$$c(x)u_k(x) = -\int_S G_i k(x-y) f_i(y)\, dS(y) \; - \int_S \sum_i jk\,(x-y) u_i(y) n_j(y)\, dS(y) \tag{4.1}$$

where

$$c(x) = \begin{cases} 1 & \text{x} \in \Omega \\ \frac{1}{2} & \text{x} \in \text{S} \end{cases}$$

and Ω is the domain of the problem (which the swimmer occupies our case) with boundary S. G is the Green's function and it can be expressed as: $G_{ij}(x) = \frac{1}{8\pi\mu}\left(\frac{\delta_i j}{|x|} + \frac{x_i x_j}{|x|^3}\right)$, $x \in \mathbb{R}^3$. $\sum$ is the Stokes-stresslet and it is represented as: $\sum_{ijk}(x) = -\frac{3}{4\pi}\frac{x_i x_j x_k}{|x|^5}$. f is the surface traction.

The first integral is known as the single layer potential, and the second integral is the double layer potential.

Moving on from the general case to our particular case, we know that for the volume changing euglenids, $\dot{V} = \int_\Gamma \ v_n^s \, dS \ \neq 0$. The total normal fluid velocity will include the permeation contribution v_n^p in order to satisfy the balance of mass of the internal fluid. The expression $\int_\Gamma \ v_n^p \, dS \ = -\dot{V}$ is then associated with the permeation contribution. The total fluid velocity at the surface is then $v^{out} = (v_n^s + v_n^p)n + ve + (v_\theta + \omega r)e + V_c e_z$. In this formula ω is the rigid body rotational velocity and V_c is the translational velocity. In terms of simplicity, a uniform field $v_n^p = -\dot{V}/S$ is the best choice, but it can also be defined as $v_n^p(u,t) = -\dot{V}(u,t)$ where h(u,t) us a profile with unit integral over the surface.[17] The interior part of the swimmer has been ignored in my study. The linear velocity along z and the azimuthal spin of the cell are calculated from the self-propulsion condition.

For swimmer immersed in a Newtonian fluid with low Reynolds number, we use a boundary integral formulation as seen in Eq. 4.1. This means the following equations are satisfied by the velocity of the fluid at any point x:

$$v_i(x) + \int_\Gamma \ T_{ijk}(x-y) v_j^{inn}(y) n_k(y) \, d\Gamma_y \ = \int_\Gamma \ G_{ij}(x-y) f_j^{inn}(y) \, d\Gamma_y \quad (4.2)$$

for $x \in \Omega$

$$v_i(x) + \int_\Gamma \ T_{ijk}(x-y) \, v_j^{out}(y) \, n_k(y) \, d\Gamma_y \ = \int_\Gamma \ G_{ij}(x-y) \, f_j^{out}(y) \, d\Gamma_y \quad (4.3)$$

for $x \in R^3 \setminus \Omega$

$f^{inn}(y)$ and $f^{out}(y)$ are the inner and outer tractions at $y \in \Gamma$ defined as $f^{inn}(y) = \sigma^{inn}(y)n(y)$ and $f^{out}(y) = -\sigma^{out}(y)n(y)$, where n(y) is the outer unit normal to $\partial\Omega$ at the point y, σ is the Cauchy stress in the fluid. G and T are the Green's functions defined earlier in this chapter.

Using the symmetry of the domain, we obtain the Fredholm integral equations for the unknown tractions f^{inn} and f^{out}, which we solve by means of the Galerkin boundary element method.[18]

If we ignore the inner behaviour of the swimmer is equivalent to equating the Dirichlet boundary conditions for the inner velocity v^{inn} to 0. The inner part of the swimmer has a traction f^{inn} equal to 0, which means it does not contribute to the motion of the dissipation of the body.[19]

[17] Arroyo, loc. cit.
[18] *Ibid.*,p. 6
[19] Arroyo,loc. cit.

The total viscous force and torque are reduced by the conditions of self-propulsion imposed, returning V_c and ω, the rigid body translational and rotational velocities. The only two important equations are:

$$\begin{array}{rcl} e_z \cdot int_\Gamma \ (f^{inn}(y) + f^{out}(y))\, d\Gamma_y & = & 0 \\ e_z \cdot int_\Gamma \ (y-o) \times (f^{inn}(y) + f^{out}(y))\, d\Gamma_y & = & 0 \end{array} \tag{4.4}$$

o is a point on the symmetry axis of the swimmer. Another hydrodynamic parameter that has been calculated was the power dissipated through the flow induced in the inner and outer flow [20]:

$$\begin{array}{rcl} W^{inn}(t) & = & \int_\Gamma \ f^{inn}(y,t) \cdot v(y,t)\, d\Gamma_y \\ W^{out}(t) & = & \int_\Gamma \ f^{out}(y,t) \cdot v(y,t)\, d\Gamma_y \end{array} \tag{4.5}$$

This helps obtain the average power exerted by the swimmer on the surrounding fluid P^{out} and average ambient fluid dissipation $P^{int+out}$:

$$\begin{array}{rcl} P^{out} & = & \int_0^T \ W^{out}(t)\, dt \\ P^{inn+out} & = & \frac{1}{T} \int_0^T \ (W^{inn}(t) + W^{out}(t))\, dt \end{array} \tag{4.6}$$

where T is the duration of a stroke.

We basically evaluate the swimming performance with the linear displacement in one stroke U, measured in units of body length $2R = sqrt\frac{S}{\pi}$, and the Lighthill's efficiency Eff_L, as mentioned in the article [21]. I have spoken more about Lighthill's efficiency in the first chapter of my thesis. For our swimmer it is defined as $\mathrm{Eff}_L^{out} = 6\pi\eta RW^2/P^{out}$ where η. Although the efficiency of metaboly is quite good, the setback of this form if movement is its relatively slow speed, approximately 1-2 μm/s, significantly less than the one of the ciliates and flagellates. An interesting conclusion that the article comes to is the fact that the swimming performance is proportional to the maximum pellicle shear. This is why I have especially focused on experimenting with different shapes, trying to optimize the efficiency.

The azimuthal energy dissipation in the fluid takes a toll on the swimmer's efficiency, which accounts for about 20% of the outer dissipation.

The distinction which has to be made while analyzing the swimmer's motion is between a power stroke and a recovery stroke. The power stroke is the motion which propels the swimmer forward, appearing as a bulge which travels downwards along the pellicle down to the tip, with striking similarity to a peristaltic wave. At the opposite pole is the recovery stroke, which pushes the swimmer backwards again, making the bulge appear at the other

[20] Arroyo, loc. cit.

[21] Arroyo,loc. cit.

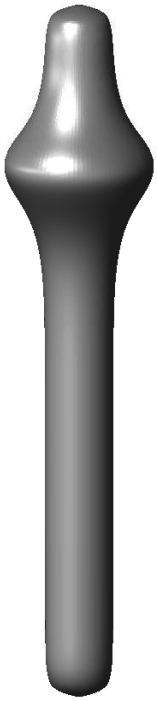

Figure 4.1: The shape of the pellicle used in the Hydrodynamics chapter

end of the pellicle. In my model, the swimmer is only performing the power stroke.

To better illustrate the capabilities of the pellicle and obtain more meaningful results, I have decided on using a slightly modified shape for the results section. The shape is presented in Fig. 4.1.

4.2 Results

I have discussed the theoretical part behind the hydrodynamics of the pellicle in the previous section. In the code, this part of the analysis has been concentrated in a solver which uses dynamic libraries. The inputs for this are: the control points, the final generating curve, a Matlab file which contains auxiliary calculations and the velocities at Gauss points.

The solver returns the total stress jump per unit area that a swimmer has to apply to reach the given velocity, the traction, the rigid body translation

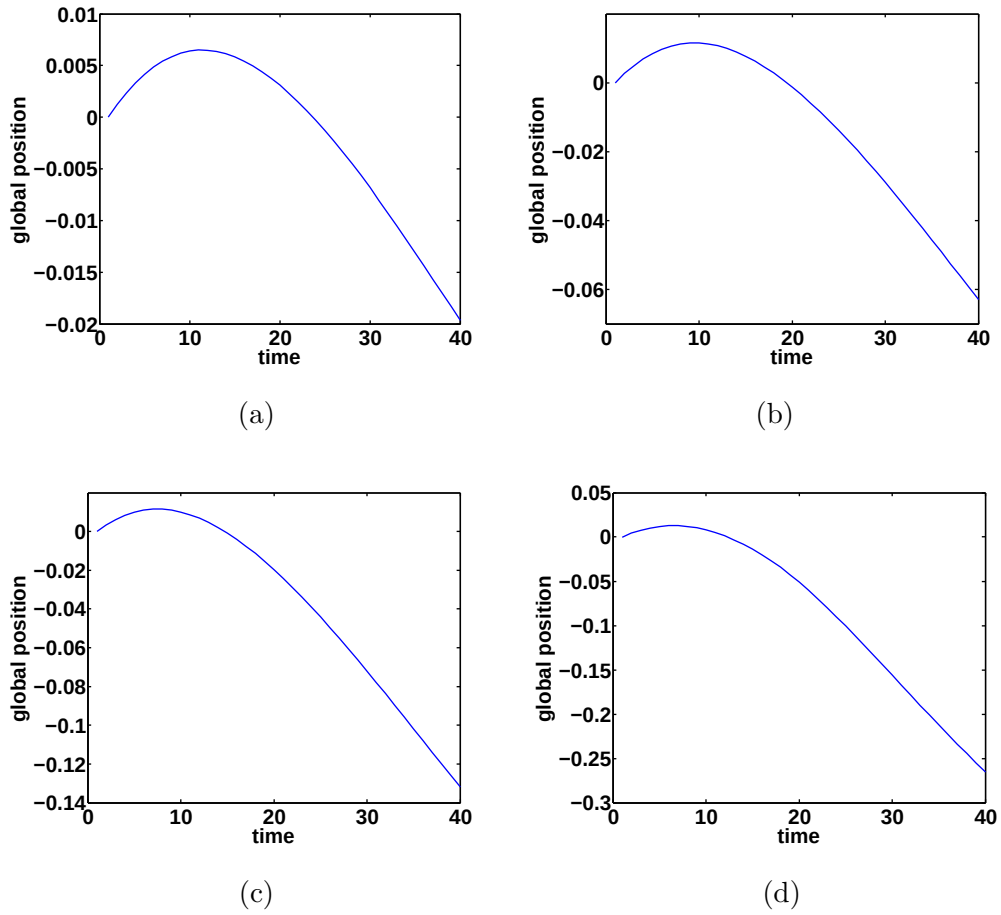

Figure 4.2: The global position with respect to different amplitudes for k = 30

and rotation velocity P_{dot} etc. I have used the velocity to calculate the global position, which basically shows us the path of the swimmer over a certain time span. $GP = \frac{t_i - t_{i-1}}{2 \cdot (\dot{T}_i + \dot{T}_{i-1})}$ where $\dot{T}$ is the translation velocity and t is the time. We also calculate the global angle, which is in fact the angular velocity: $GA = \frac{t_i - t_{i-1}}{2 \cdot (\dot{R}_i + \dot{R}_{i-1})}$. When plotted, the global position should be a smooth line.

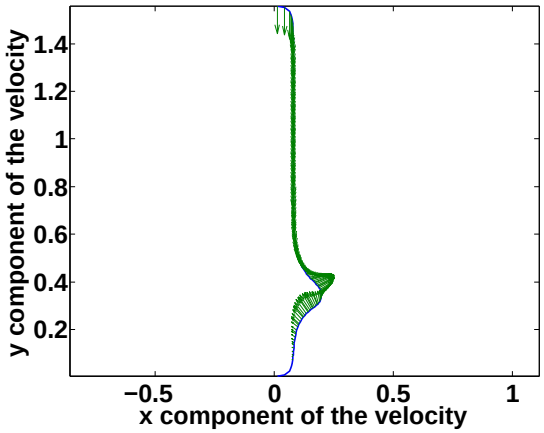

(a) In plane velocity at time step 1

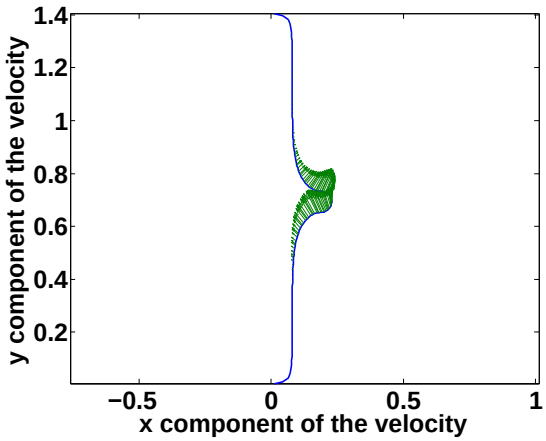

(b) In plane velocity at time step 20

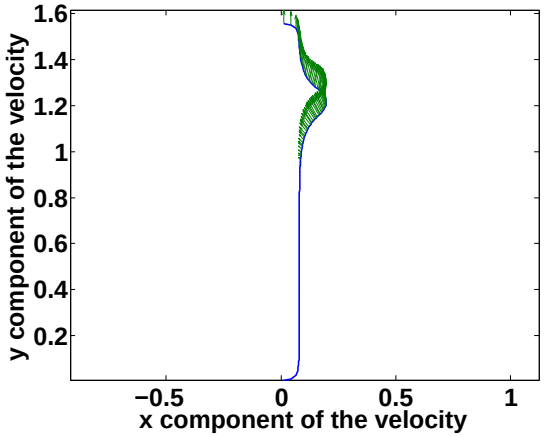

(c) In plane velocity at time step 40

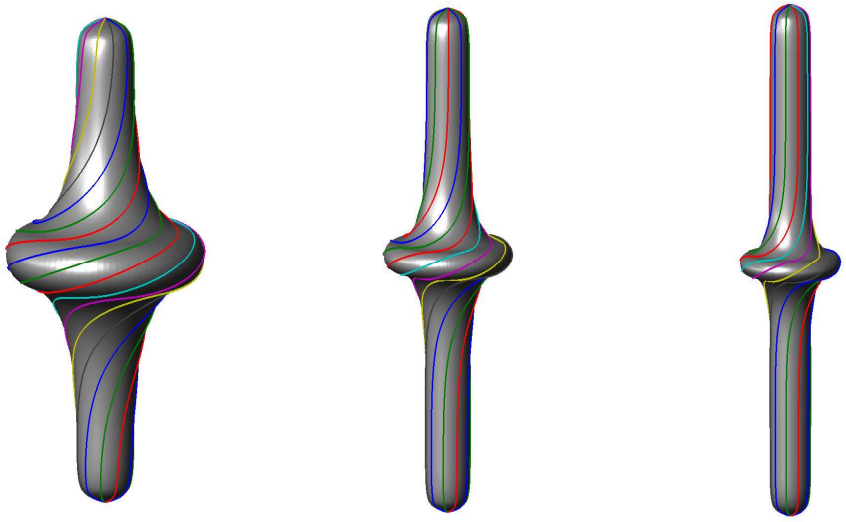

(d) k = 10, amp. = 3.57 (e) k = 30, amp. = 2.91 (f) k = 60, amp. = 2.5

Figure 4.3: The deformed pellicle for the 3 different bulge widths, inversely proportional to parameter k from Eqs. 4.7 and 4.8 and for the maximum amplitude possible in each situation.

The calculations behind the hydrodynamic solver can be divided into two parts based on the type of movement of the pellicle: translation and rotation. For the translation part such parameters as the translation drag and the total force are obtained which lead to getting the translation velocity which is Total force/Translation drag.

For the rotation part, on the other hand, the solver processes the values for the rigid torque and the total torque which once divided, give us the angular velocity. The translation and angular velocity are useful in calculating the global velocity and the global angle, as I have previously shown.

To remind the reader, the shear function I have used in my computations and its derivative are:

$$\gamma_{CP3} = amplitude \cdot e^{-k\cdot((u_{CP}-0.5)-0.5\cdot(t-0.5))^2}; \tag{4.7}$$

$$\dot{\gamma}_{CP3} = k \cdot ((u_{CP} - 0.5) - 0.5 \cdot (t - 0.5)) \cdot \gamma_{CP}; \tag{4.8}$$

From Figure 4.2 we can see the relationship between the amplitude and the global position of the swimmer. We can define the maximum admissible shear as the value where the shear representation does not make any physical sense. The maximum amplitudes for which the model works, but is at the maximum admissible shear are different for different sizes of the bulge, as seen in Table 4.1.

K (1/width)	Amplitude	Lighthill Efficiency(%)	Norm. Vel.
10	0.89	0.9651	0.0607
	1.80	6.33	0.1746
	2.70	15.56	0.3310
	3.57	25.4332	0.5667
30	0.72	0.2506	0.0349
	1.40	1.3831	0.1119
	2.10	4.3229	0.2344
	2.91	10.0622	0.4716
60	0.62	0.1203	0.0217
	1.2	0.6290	0.0745
	1.8	2.0495	0.1688
	2.5	5.2777	0.3629

Table 4.1: Table showing the maximum Lighthill Efficiency for different solvers and shapes.

I have computed the Lighthill Efficiency and the normalized velocity for 3 different bulge widths and 4 amplitudes for each bulge. This shows the influence of the bulge width and amplitude on the results. The results are visible in Table 4.1 and they denote the fact that with a wider bulge the locomotion is more efficient and the euglenid moves at a higher velocity. This is a confirmation of what I have stated previously: the more the pellicle deforms, the more the swimmer advances.

Chapter 5

Conclusions

The results that I came to during my research show a consistency with what has been shown in the article by Arroyo *et al.*[1]. My purpose from the very beginning was to numerically analyze the movement, so I did just that, parametrizing the movement in a numerical model and finalizing by 'releasing' the model of the swimmer in a newtonian fluid and doing the subsequent hydrodynamical calculations.

The pellicle shear amplitude influences what is known in my study as the global position of the swimmer, which is the translation velocity in time. In layman's terms, this means that the more the pellicle bends, the more the euglena advances. My model has shown high adaptability, as the shape can be easily molded, and as you have seen in my previous figures, there are numerous ways to play with the parameters and obtain interesting results.

Taking into account the fact that the Reynolds number for a euglenoid swimming in water is about 10^{-4} dyn, which can be converted to 10^{-9} N, the efficiency of the movement is good, even compared to microorganisms which use a flagella or cillia. For a wide bulge traveling across the length of the euglenid, the Lighthill efficiency can reach a percentage of 25 %, which is the maximum value I was able to obtain as seen in Table 4.1. As for the normalized velocity, it increases in the same manner as the Lighthill Efficiency.

Metaboly is composed of two motions: the power stroke and the recovery stroke. During the recovery stroke, the swimmer loses some of the advantage gained in the power stroke. My model only executes the power stroke, which explains the very high Lighthill Efficiency values obtained.

One of the reasons euglenoids have developed this kind of motility is the fact that they are usually found in granular substrates, where using the flagellum for propulsion is very difficult.

The green euglena might be a minute creature which cannot even be seen

with the naked eye, but its complex pellicle holds a lot of information that can lead to breakthroughs in many fields. As good idea for future studies on the euglenoid pellicle is, as I have mentioned before, applying it in the field of microfluidics, and specifically in the case of peristaltic micropumps or microvalves.

I will conclude my exposition on the mechanics behind the locomotion of the green euglena by expressing my newfound fascination for the possibilities offered by the study of microorganisms such as the green euglena and hope that it will prove useful in many fields of work. As the romans once said *natura nihil frustra facit*, meaning nature does nothing in vain. There is always something left to learn by looking at the nature surrounding us and this feeds the inquisitive minds of scientists everywhere.

Bibliography

[1] Arroyo M., Heitai L., Millan D., DeSimone A.(2012) Reverse engineering the euglenoid movement. *PNAS* 109: 17874-17879.

[2] Purcell E.M.(1977) Life at low Reynolds numbers. *Am J Phys* 45:3-11.

[3] Lauga E., Powers T.R.(2009) The hydrodynamics of swimming microorganisms. *Rep. Prog. Phys.* 72:096601.

[4] Osterman N., Vilfan A.(2011) Finding the ciliary beating pattern with optimal efficiency. *PNAS* 38:15727-15732.

[5] Leander B.S. (2008) Euglenida,euglenids or euglenoids. Version 11 September 2008.¡2008.09.11 in The Tree of Life Web Project¿.

[6] Leander B.S., Witek R.P., Farmer M. A.(2001) Trends in the evolution of the euglenid pellicle. *Evolution* 55:2215-2235.

[7] Suzaki T., Williamson R.E.(1985) Euglenoid movement in euglena fusca: Evidence for sliding between pellicular strips. *Protoplasma* 124:137-146.

[8] Lukes J., Leander B.S., Keeling P.J.(2009) Cascades of convergent evolution: The corresponding evolutionary histories of euglenozoans and dinoflagellates. *PNAS* 106:9963-9970.

[9] Lighthill J.(1975) Flagellar Hydrodynamics: The John von Neumann Lecture. *SIAM Review* 2:161-230.

[10] Stone H.A., Samuel A.D.T.(1996) Propulsion of microorganisms by surface distortions. *Phys Rev Lett* 77:4102-4104.

[11] Avron J.E., Gat O., Kenneth O.(2004) Optimal swimming at low Reynolds numbers. *Phys Rev Lett* 60:469-486.

[12] Alouges F., Heltai L. (2011) Numerical strategies for stroke optimization of axisymmetric microswimmers. *Math Mod Meth Appl S* pp. 361-387.

[13] Najafi A., Golenistan R. (2004) Simple swimmer at low Reynolds number:Three linked spheres. *Phys Rev E* 69:062901.

[14] Arroyo M., Ortiz M. (2006) Local maximum-entropy approximation schemes: a seamless bridge between finite element and meshfree methods. *Int J Numer Meth Eng* 65:2167-2202.

[15] Pozrikidis C. (1992) *Boundary integral and singularity methods for linearized viscous flow* , Cambridge Texts in Applied Mathematics. (Cambridge University Press, Cambridge).

[16] Marsden J, Hughes T.(1983) *The mathematical foundations of elasticity* . (Prentice-Hall).

[17] Tenenbaum J.B., Silva V., Langford J. C. (2000) A global geometric framework for nonlinear dimensionality reduction. *Science* 290:2319-2323.

[18] do Carmo M.(1976) *Differential geometry of curves and surfaces.* (Prentice-Hall).

[19] Piegl L., Tiller W.(1997) *The NURBS Book.* (Springer).

[20] Fletcher D.A., Theriot J. A.(2004) An introduction to cell motility for the physical scientist. *Phys Biol* 1:T1-T10.

[21] Dobell C.(1932) *Antony van Leeuwenhoek and his "Little Animals".* (Dover, New York).

[22] Avron J.E., Kenneth O, Oaknin D.H. (2005) Pushmepullyou: an efficient microswimmer. *New J Phys* 7:234.

[23] Leander B.S., Esson H.J., Breglia S.A. (2007) Macroevolution of complex cytoskeletal systems in euglenids. *BioEssays* 29:987-1000.

[24] Suzaki T., Williamson R.E. (1986) Cell surface dislacement during euglenoid movement and its computer simulation. *Cell Motil Cytoskel* 6:186-192.

[25] Suzaki T., Williamson R.E. (1986) Reactivation of the euglenoid movement and flagellar beating in detergent-extracted cells of astasia longa: different mechanisms of force generation are involved. *J Cell Sci* 80:75-89.

[26] Triemer R.E. (1999) The euglenoid project. .

[27] Stephens G.J., Johnson-Kerner B., Bialek W., Ryu W.S. (2008) Dimensionality and dynamics in the behaviour of C. Elegans. *PLoS Comput Biol* 4:e1000028.

[28] Stephens G.J., Osborne L.C., Bialek W. (2011) Searching for simplicity in the analysis of neurons and behaviour. *Proc Natl Acad Sci USA* 108:15565-15571.

[29] Holzapflel G.A. (2000) *Nonlinear Solid Mechanics: A Continuum Approach for Engineering.* (Wiley).

[30] Toba S., Watanabe T.M., Yamaguchi-Okimoto L., Toyoshima Y.Y., Higuchi H. (2006) Overlapping hand-over-hand mechanism of single molecular motility of cytoplasmic dynein. *Proc Natl Acad Sci USA* 103:5741-5745.

[31] Carter N.J., Cross R.A. (2005) Mechanics of the kinesin step. *Nature* 435:308-312.

[32] Katsu-Kimura Y., Nakaya F., Baba S.A., Mogami Y. (2009) Substantial energy expenditure for locomotion in ciliates verified by means of simultaneous measurement of oxygen consumption rate and swimming speed. *J Exp Biol* 212:1819-1824.

[33] Alouges F., DeSimone A., Lefebvre A. (2008) Optimal strokes for low Reynolds number swimmers: an example. *J Nonlinear Sci* 18:277-302.

[34] Gebeshuber I.C., et al. (2009) *Bio-Inspired Nanomaterials and Nanotechnology* , ed. Zhou Y. (Nova Science).

[35] Drescher K, et al. (2009) Dancing volvox: Hydrodynamic bound states of swimming algae. *Phys Rev Lett* 102:168101.

[36] Spagnolie S. E., Lauga E. (2010) Jet propulsion without inertia. *Phy Fluids* 22:081902.

[37] Liu B., Powers T.R., Breuer K.S. (2011) Force-free swimming of a model helical flagellum in viscoelastic fluids. *Proc Natl Acad Sci USA* 108:19516-19520.

[38] Esson H.J., Leander B.S. (2008) Novel pellicle surface patterns on euglena obtusa (euglenophyta) from the marine benthic environment: Implications for pellicle development and evolution. *J Phycol* 44:132-141.

[39] Spagnolie S.E., Lauga E. (2010) The optimal elastic flagellum. *Phys Fluids* 22:031901.

[40] Tam D., Hosoi A.E. (2011) Optimal feeding and swimming gaits of biflagellated organisms. *Proc Natl Acad Sci USA* 108:1001-1006.

[41] Fletcher D.A., Geissler P.Ñ. (2009) Active biological materials. *Annu Rev Phys Chem* 60:469-486.

[42] Klein Y., Efrati E., Sharon E. (2007) Shaping of elastic sheets by prescription of non-euclidean metrics. *Science* 315:1116-1120.

[43] Bhattacharya K., DeSimone A., Hane K.F., James R.D., Palmstrom C. (1999) Tents and tunnels on martensitic films. *Mat Sci Eng A-Struct* 273-275:685-689.

[44] Bhattacharya K., James R.D. (2005) The material is the machine. *Science* 307:53-54.

[45] Kostyuchenko V.A., et al. (2005) The tail structure of bacteriophage t4 and its mechanism of contraction. *Nat Struct Mol Biol* 12:810-813.

[46] Zhu L., Lauga E., Brandt L. (2013) Low-Reynolds number swimming in a capillary tube. *J Fluid Mech* 726:285-311.

[47] Ramia M., Tullock D.L., Phan-Thien N., (1993) The role of hydrodynamic interaction in the locomotion of microorganisms. *Biophys J* 65:755-778.

[48] Shum H., Gaffney E.A., Smith D.J. (2010) Modelling bacterial behaviour close to a no-slip plane boundary: the influence of bacterial geometry. *Proc R Soc* A466:1725-1748.

[49] Stam J., Schmidt R. (2011) On the Velocity of an Implicit Surface. *ACM Transactions on Graphics* 21(3):21.

[50] Lai T.L., Robbins H., Wei C.Z. (1978) Strong consistency of least squares estimates in multiple regression. *Proc Natl Acad Sci USA* 75(7): 3034–3036.